Hindawi Publishing Corporation
Journal of Nanomaterials
Volume 2011, Article ID 865969, 11 pages
doi:10.1155/2011/865969

Review Article

Atoms and Nanoparticles of Transition Metals as Catalysts for Hydrogen Desorption from Magnesium Hydride

N. Bazzanella, R. Checchetto, and A. Miotello

Dipartimento di Fisica Università degli Studi di Trento, 38123 Povo, Italy

Correspondence should be addressed to A. Miotello, antonio.miotello@unitn.it

Received 9 April 2010; Accepted 18 August 2010

Academic Editor: Bo Zou

The hydrogen desorption kinetics of composite materials made of magnesium hydride with transition metal additives (TM: Nb, Fe, and Zr) was studied by several experimental techniques showing that (i) a few TM at.% concentrations catalyse the H_2 desorption process, (ii) the H_2 desorption kinetics results stabilized after a few H_2 sorption cycles when TM atoms aggregate by forming nanoclusters; (iii) the catalytic process occurs also at TM concentration as low as 0.06 at.% when TM atoms clustering is negligible, and (iv) mixed Fe and Zr additives produce faster H_2 desorption kinetics than single additive. The improved H_2 desorption kinetics of the composite materials can be explained by assuming that the interfaces between the MgH_2 matrix and the TM nanoclusters act as heterogeneous sites for the nucleation of the Mg phase in the MgH_2 matrix and promote the formation of fast diffusion channels for H migrating atoms.

1. Introduction

Because of the high hydrogen storage capacity of MgH_2, ~7.6 wt.%, low cost, and weight, magnesium is still currently investigated for H_2 storage applications. Most research efforts are dedicated to the improvement of the kinetic H_2 sorption process that is too slow even at temperatures larger than 500 K. The hydrogen desorption process results from many single steps taking place in series: the nucleation of the Mg phase in the MgH_2 parent phase and the diffusion of hydrogen atoms through transformed Mg and/or not transformed MgH_2 layers to the sample surface where the H_2 recombitative desorption occurs. The velocity of these reaction steps could be limited by the surface Mg oxide layer impeding the H_2 surface processes [1, 2] or by the presence of a continuous MgH_2 layer acting as hydrogen diffusion barrier [3]. On the contrary, the hydrogen absorption and desorption kinetic in Mg can be improved by microstructural refinements such as the reduction of the Mg or MgH_2 grain size: grain boundaries are, in fact, active nucleation sites for the formation or dissociation of the hydride phase and act as preferential diffusion paths for H atoms [4]. The major improvements are generally obtained by the use of a proper metal or metal oxide additive. Transition metals or transition metal oxides additives favour the H_2 dissociation [5] and can further improve the H_2 sorption kinetics in different ways. Nanocomposite materials formed by milling MgH_2 and Nb or Nb oxide powders are the most studied systems. Time-resolved X-rays synchrotron analysis suggested the transformation during H_2 desorption at 573 K of the NbH nanocatalyst in the metastable, H vacancy rich $NbH_{0.6}$ phases: the catalytic effect was thus explained as an enhanced transfer of H atoms from the MgH_2 matrix to the Mg surface by H diffusion through the catalyst layers [6]. Recent studies on the structural analysis of MgH_2 samples catalysed by Nb [7] or Nb oxides [8] suggest the formation of Mg-Nb perovskite phases by reaction of Nb_2O_5 and Mg: the perovskite was suggested to act as preferential "pathways" for hydrogen diffusion.

We have recently studied the H_2 desorption process from MgH_2 samples where the metallic additives, single or mixed atomic species, were completely included inside the MgH_2 matrix [9–15]. These samples allow to specifically investigate the role of the additives, in the bulk processes, leading to

the decomposition of MgH_2 phase and to the H_2 desorption process. In this paper we present a comprehensive review of our experimental results.

In particular, in Section 2 we review the studies on the hydrogen desorption kinetics from pure and Nb-catalysed MgH_2, and then we discuss the role of the Nb additive when it is distributed inside the MgH_2 matrix at concentration ranging from <0.1 to about 5 at.%.

In Section 3 we will present the results of the experimental analysis dedicated to the structural and chemical-physical characterization of the Nb additive when dispersed in the Mg or MgH_2 matrix.

In Section 2 we present a study on the comparison between the catalytic effect of different TM additives contained inside the MgH_2 matrix at concentration ~5 at.%.

Finally, in Section 3, we will present results on a novel route to enhance the hydrogen desorption kinetics from MgH_2 by using mixed TM additive.

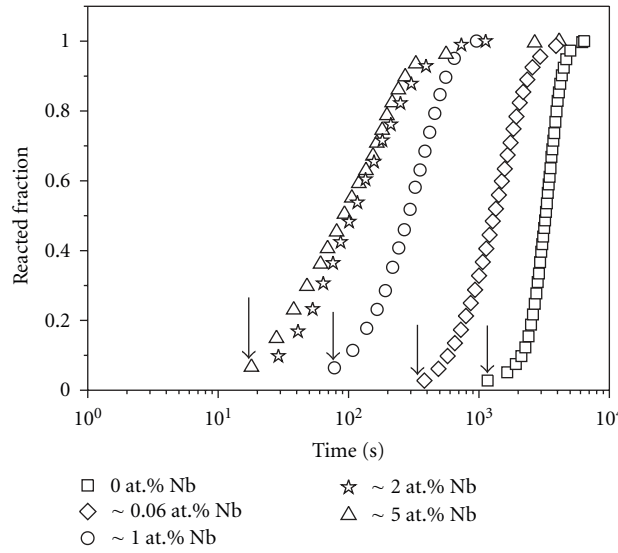

Figure 1: Hydrogen desorption kinetics at 623 K from MgH_2 samples with different Nb concentrations.

2. Hydrogen Desorption Properties of Nb-Doped MgH_2 Samples

Samples of pure Mg and Nb-doped Mg with different concentrations of Nb (see Table 1) were deposited by RF magnetron sputtering in form of films with thickness ~10–20 μm on 5 cm diameter polished graphite wafers. The Nb doping was obtained by putting a few numbers of small Nb fragments on the surface of Mg target in such a way that sputtering process involves both Mg and Nb, that is, a co sputtering procedure was utilized to prepare Mg-doped samples [9]. To prevent the surface oxidation and stimulate the H_2 dissociation at the Mg surface, samples were coated with a 15 nm thick Pd capping layer without interrupting the vacuum conditions in the deposition chamber. Pd is known to split hydrogen, and splitting is an important step in the hydrogen sorption process though it might be not the rate-limiting step. Indeed, at temperatures larger than 250–300 K, Pd is transparent to hydrogen [16].

The Nb concentration was measured, after deposition, by Energy Dispersion Spectroscopy (EDS) while Secondary Ions Mass Spectroscopy (SIMS) was employed with samples having Nb concentration lower than 1 at.% and to verify the uniform distribution of the Nb catalyst into the Mg layers [12]. After deposition, Mg samples peeled off from the substrate and the self-supporting samples were introduced in a Sievert-type apparatus to study the hydrogen absorption and desorption kinetics: details on the sample preparation, activation procedure, and experimental analysis are described elsewhere [9, 17].

In Figure 1 we present the hydrogen desorption kinetics from MgH_2 at 623 K in samples having different Nb concentrations. The figure shows a strong increase of the reaction velocity for all the Nb-doped Mg: the reaction half-time $\tau_{1/2}$, that is the interval time needed to have half of MgH_2 transformed to h-Mg, decreases from 3250 ± 50 s for pure MgH_2 to 110 ± 10 s for the 2-to-5 at.% Nb-doped MgH_2. Intermediate values of $\tau_{1/2}$ are observed at lower Nb concentrations: 290 ± 10 s for 1 at.% and 2390 ± 30 s for 0.06 at.%. A corresponding reduction of the incubation time, that is the typical time needed for the nucleation of the Mg phase, can also be observed in Figure 1 (arrows indicate the reacted fraction firstly evidenced that roughly corresponds to the incubation time).

The desorption processes of Figure 1 have been satisfactorily described in the framework of the Johnson-Mehl-Avrami theory for solid-state transformation [18]. The relevant effective parameters of the model, say, the values of the reaction order, n, and activation energy, E_a, are reported in Table 1. The obtained different values suggest that different mechanisms control the H_2 desorption kinetics at different Nb concentrations.

The value $n = 4$ obtained for pure MgH_2 indicates that the continuous formation of stable Mg nuclei in the MgH_2 parent phase is the rate-limiting step in the H_2 desorption kinetics. $n = 1$ for MgH_2 samples with Nb content of 2–5 at.% indicates an instantaneous nucleation of the Mg metallic phase in the MgH_2 followed by its diffusional growth [9]. The evaluated value of the activation energy, 51 ± 5 kJ/mol H, suggests that the diffusional growth is limited by H atomic diffusion in Mg layers: this value is, in fact, close to that of the activation energy for H diffusion in bulk Mg, 40 kJ/mol H [19]. Structural analysis by X-Ray Diffraction (XRD) and Extended X-ray Absorption Fine Structure (EXAFS) [12] evidenced, as we will report below, the formation of Nb:H nanoclusters. We thus explained the kinetic results by assuming that (a) the interface between the Nb:H nanoclusters and the MgH_2 matrix offers sites where the instantaneous nucleation of the Mg phase occurs (heterogeneous nucleation) and (b) H atoms dissociated from the Mg hydride migrate to the sample surface (where desorption occurs) through domains of transformed Mg. Kinetic data presented in Figure 1 indicate that the same behaviour is shown by samples with Nb dopant concentration ≥2 at.%. This result is relevant for application because it shows that

Table 1: Evaluated values of the half-reaction time ($\tau_{1/2}$) at $T = 623$ K, order of reaction (n), and activation energy (E_a) of MgH_2 samples with different Nb concentrations.

Sample	$\tau_{1/2}$ (s)	n	E_a(kJ mol^{-1} H)
Pure Mg	3250 ± 50	4	141 ± 5
Mg + 0.06 at.% Nb	2390 ± 30	2	140 ± 5
Mg + 1 at.% Nb	290 ± 10	1.5	78 ± 5
Mg + 2 ÷ 5 at.% Nb	110 ± 10	1	51 ± 5

the optimum catalyst concentration can be lower than 5 at.%, the concentration usually reported for ball-milled Mg [20]. Note that only a few other catalysts were tested at so low concentration [21].

Relevant differences on hydrogen desorption kinetics are observed in samples with Nb concentration lower than 2–5 at.%: the kinetic curve for 1 at.% Nb concentration is reproduced with $n = 1.5$ and $E_a = 78 \pm 5$ kJ/mol H. The XRD spectrum of such sample (see [12]) shows that Nb atoms form Nb:(H) nanoclusters with size nearly equal to that observed in samples with larger Nb content. Because of the lower Nb concentration, there is thus a larger distance between the Nb:H nanoclusters and a lower specific MgH_2-Nb:H interface area as compared to the 2–5 at.% Nb-doped samples. The larger value of the activation energy (78 versus 51 kJ/mol) cannot be simply explained as an effective value describing the H_2 effusion kinetics of a material that consists of a fraction of Nb-catalysed MgH_2 and a fraction of pure MgH_2: effusion simulation carried out by assuming that the hydride consists of a larger fraction of MgH_2 with embedded Nb clusters, and a lower fraction of pure MgH_2 cannot reproduce the observed H_2 desorption kinetics. On the contrary, by assuming that the observed kinetics still obeys a diffusion-controlled kinetics, the evaluated values of $n = 1.5$ and $E_a = 78$ kJ/mol can be explained by observing that:

(a) the presence of Nb:H clusters still provide a large density of Mg phase nucleation centers with low activation energy barriers (as in the case of 5 at.% Nb); this point is confirmed by the reduced values of the incubation time when compared with the pure Mg hydride;

(b) the increased distance between the Nb clusters in the MgH_2 matrix limits the onset of interconnected Mg domains which favour the H atomic diffusion [9].

The evaluated value of the activation energy, 78 ± 5 kJ/mol H, is not much different from the value of the activation energy, 100 ± 10 kJ/mol H, for H diffusion in MgH_2 as reported by Fernández et al. [22]. This suggests that the rate-limiting step in the H diffusion is given by the energy barrier to be overcome by the migrating species in not transformed MgH_2 phase.

A final interesting result comes out from the analysis of the sample with the lower Nb concentration, 0.06 at.%. Here the clustering of the Nb atoms is a negligible process because the Nb concentration is close to the solubility limit of Nb in Mg, [Nb/Mg] ~ 10^{-4} [23]. A catalytic effect of Nb on hydrogen desorption can be still observed as indicated by the reduction of the $\tau_{1/2}$ parameter with respect to that observed in the undoped MgH_2. After repeated H_2 absorption-desorption cycles, the catalytic properties decrease and the 0.06 at.% Nb-MgH_2 exhibits a value of the $\tau_{1/2}$ parameter comparable to that of pure MgH_2 but lower incubation time. This means that the Mg nucleation process still results in acceleration. Because the relevant activation energy value of the desorption process is just the same as in the case of pure Mg (see Table 1), we may conclude that single Nb atoms may constitute seeds for heterogeneous Mg nucleation in the same way as homogeneous seeds operate in pure Mg.

In particular, we suggest that the atomic environment around the Nb impurity atom acts as nucleation seed for the Mg phase given the presence of local elastic strains due to the atomic size difference between solute (Nb) and solvent atoms (Mg, H). The decrease of the phase transition velocity after the first absorption-desorption cycles is explained by impurity segregation at extended defects, such as grain boundaries, that reduce the availability of heterogeneous nucleation seeds.

In conclusion, several different mechanisms influence the hydrogen kinetics in MgH_2 depending on the Nb atomic concentration: specifically, at concentration larger than 1 at.%, Nb forms nanoclusters that affect both the Mg nucleation process and hydrogen diffusion. At very low concentration, 0.06 at.%., Nb remains atomically dispersed (clustering of the Nb atoms should be negligible because the Nb concentration, as indicated above, is close to the solubility limit in Mg) and the only effect of Nb is on favouring the Mg-phase nucleation.

3. EXAFS and TEM Analysis of Nb-Doped MgH_2

In order to further clarify the role of the Nb doping element, we studied the evolution of the chemical-physical state of the Nb atoms dispersed in the Mg matrix upon hydrogen absorption and desorption cycles. The analyses were carried out by EXAFS, XRD, and Transmission Electron Microscopy (TEM) analysis on three representative Nb-doped Mg samples: (i) as-deposited sample, (ii) activated MgH_2 samples after partial MgH_2 to Mg phase transition (hereafter, hydrogenated sample), and (iii) activated sample after complete MgH_2 to Mg phase transition (hereafter, dehydrogenated sample). Details on the measurements and data analysis are reported in [11].

Results show that stable catalytic effects of Nb are connected with the formation of Nb nanoclusters dispersed

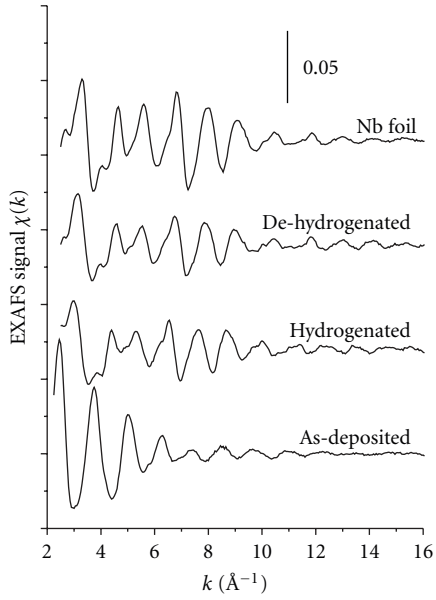

Figure 2: Nb K-edge EXAFS spectra from Nb-doped (5 at.%) Mg samples; the spectra of the hydrogenated and dehydrogenated samples are pertinent to fully activated samples.

in the Mg matrix while no evidence of Nb oxidation could be deduced from previous analysis.

In Figure 2 we present the EXAFS spectra of the samples together with the spectrum of crystalline Nb: we observe that the spectrum of the as-deposited sample is different from the spectra of the hydrogenated and dehydrogenated samples which are similar to that of crystalline Nb.

In Figure 3 we show the moduli of the Fourier transformed spectra compared with the corresponding best-fit curves of the first two interatomic correlation signals: the spectrum of the as-deposited sample differs from that of the metallic Nb; the other two are quite similar, except for the fact that for the hydrogenated sample the peaks located at about 2.7 and 3.1 Å are shifted towards higher R (the interatomic distance) values with respect to the Nb foil spectrum. The results of the EXAFS analysis are reported in Table 2.

In the as-deposited sample, the average local structure around Nb is composed mainly of Mg atoms, at a distance that is shorter with respect to the corresponding value of the crystalline Mg and appears in agreement with the first Nb-Mg coordination distance obtained by simulating an Nb substitutional impurity in an Mg cluster. Besides this main signal, the analysis evidenced also an Nb-Nb correlation, as shown in Figure 3(b), where in the backtransformed k-space the filtered data and fit are compared and the different contributions to the fit are reported. The Nb-Nb correlation indicates the presence of Nb aggregates: the fact that the coordination number is low (about 1) and the Nb-Nb distance is shorter than for the bulk Nb strongly suggests that the clusters are composed of few Nb atoms. In the hydrogenated sample, the Nb-Mg signal is below the detectable limit; two Nb-Nb correlations are evident indicating the presence of Nb-containing nanoclusters: the Nb-Nb distances are ~4.5% longer than the corresponding values in crystalline Nb. We ascribe this fact to the presence of H atoms into the Nb clusters increasing the interatomic distance: the local structure around Nb is in agreement with both the αNb-H phase (with an H/Nb atomic ratio of 0.9) [24] and with the orthorhombic βNb-H phase (with an H/Nb atomic ratio higher than 0.8) [25]. It is worth noting that the coordination number is lower than the corresponding value in the bulk Nb, due to the fraction of Nb atoms located on the cluster surface and, possibly, to Nb atoms dispersed in the Mg matrix. After the hydrogen desorption process, the Nb is still aggregated in nanoclusters: in this case, the Nb-Nb coordination distances are those of the corresponding bulk phase: this indicates the H desorption from the Nb clusters (see [6] to gain insight on formation, decomposition, and general features on stability of NbH). The fact that the coordination numbers in this case are even lower than those of the hydrogenated sample could likely indicate a smaller size of the nanoclusters and/or a larger fraction of Nb atoms dispersed into the Mg matrix. As in the hydrogenated sample, the Nb-Mg signal is below the detectable limit for the EXAFS spectroscopy.

The XRD spectrum of the as-deposited sample [9] shows a preferential growth of the Mg film with the (0001) planes parallel to the substrate. After hydrogenation, the sample shows a complex pattern formed of many peaks; see Figure 4: the peaks can be attributed to a tetragonal MgH_2 phase with lattice parameters $a = 0.4517$ nm and $c = 0.30205$ nm (ICDD card n. 12-697) and to an orthorhombic β-$NbH_{0.89}$ phase with lattice parameters $a = 0.484$ nm, $b = 0.490$ nm, and $c = 0.345$ nm (ICDD card n. 7-263). The unindexed peaks are due to Mg layers that have lost the absorbed hydrogen. The mean grains size of the β-$NbH_{0.89}$ phase, estimated by using the Scherrer equation after deconvolution of the Mg(101) and $NbH_{0.89}$(200) peaks, see the inset of Figure 4, is ~20 nm. The presence of metallic Nb was never detected in the hydrogenated sample. The dehydrogenated sample shows a very simple XRD pattern where, apart from the unindexed Mg peaks, only the first three peaks of metallic Nb (bcc, $a =$ 0.33066 nm, ICDD card n. 35-789) are present; see Figure 5. The mean grains size of the metallic Nb, calculated from the measurement of the FWHM of the Nb(110) peak, is ~15 nm. It is worth to note that in this case the Mg- and Nb-hydrides are completely disappeared.

TEM observations performed on the as-deposited sample evidenced the preferential growth of the film, in agreement with the XRD results, as well as the absence of any nanocluster or precipitate inside the Mg grains. The size of these grains ranges from 0.1 to 1.5 μm. The electron diffraction pattern has a ring structure attributable to Mg. In this case, the few-atom aggregates detected by the EXAFS spectroscopy are most likely too small to give a significant contribution to the whole diffraction pattern. A completely different appearance is shown by the hydrogenated sample: spherical nanoclusters with dimensions ranging from 5 to 25 nm, not uniformly dispersed inside the grains, are clearly visible after few minutes of permanence under the electron

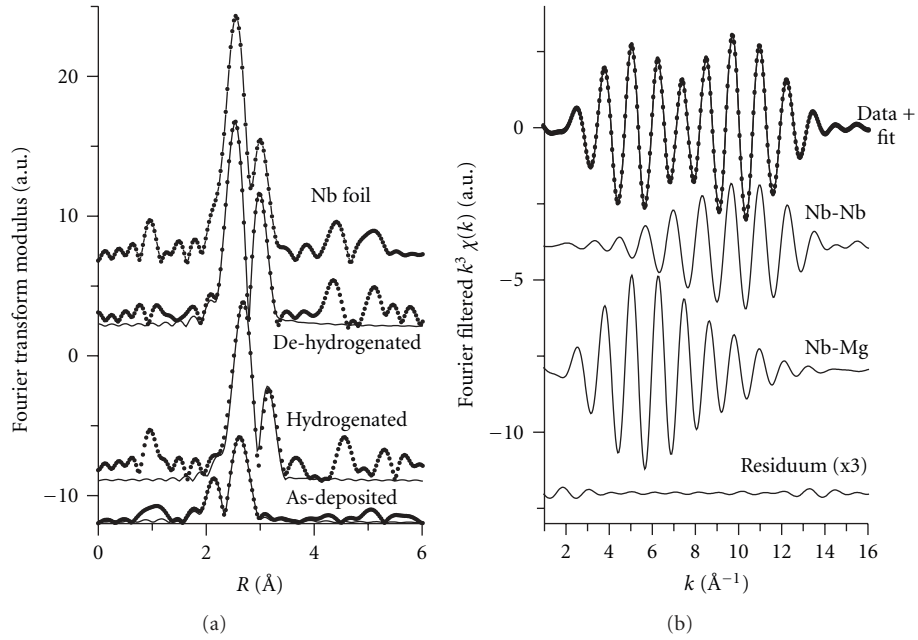

Figure 3: EXAFS analysis of the Nb-doped (5 at.%) Mg samples. (a) k^3-weighted Fourier transform moduli (transformation range k = 3–13 Å^{-1} for the as-deposited sample, k = 3–16 Å^{-1} for the others) of the EXAFS spectra (markers) and corresponding best-fit curves (solid line) of the first two coordination signals (Nb-Mg and Nb-Nb for the as-deposited sample, two Nb-Nb for the others); no back-scatterer phase-shift correction was applied in the figure. (b) Fourier filtered spectrum (markers) in the fitting range and superimposed fit (solid line) of the as-deposited EXAFS spectrum; the residuum and the two single-scattering signals that contribute to the fit are reported.

Table 2: Results of the Nb K-edge EXAFS analysis on Nb-doped Mg films; for each pair of atoms, N is the coordination number, R the interatomic distance, and σ^2 the Debye-Waller factor. The uncertainty in the fitting results corresponds to a confidence level of 68%. Crystallographic data for metallic Nb and the simulation of the local structure around an Nb substitutional impurity into the Mg lattice are also reported.

Sample		N	R (Å)	σ^2 (10^{-4} Å^2)
As-deposited	Nb-Nb	1.2 ± 0.4	2.73 ± 0.01	38 ± 9
	Nb-Mg	9.6 ± 0.9	3.08 ± 0.01	99 ± 8
Hydrogenated	Nb-Nb	5.6 ± 0.3	3.00 ± 0.02	57 ± 6
	Nb-Nb	4.2 ± 0.2	3.45 ± 0.02	66 ± 8
dehydrogenated	Nb-Nb	4.0 ± 0.2	2.87 ± 0.01	44 ± 4
	Nb-Nb	3.0 ± 0.2	3.32 ± 0.01	40 ± 4
metallic Nb	Nb-Nb	8	2.8638	
	Nb-Nb	6	3.3068	
Nb-doped Mg (simulation)	Nb-Mg	6	3.075	
	Nb-Mg	6	3.195	

beam (a longer permanence induces the decomposition of the Mg- and Nb-hydrides). The electron diffraction pattern of the sample only shows the presence of Mg rings and a very weak ring attributable to metallic Nb. Finally, the dehydrogenated sample is stable under the electron beam, and its structure is formed of spherical nanoclusters with dimensions in the range 10–20 nm. These nanoclusters are not uniformly distributed inside the grains; see Figure 6, where the Nb particles appear as small black dots. The electron diffraction pattern of this sample is formed of spotty rings due to Mg and few well evident extra spots due to metallic Nb.

The present structural analysis thus shows that the accelerated H_2 desorption kinetics is connected to the presence of the Nb nanoclusters [12]. As suggested by the analysis of the desorption curves, the role of the nanoclusters is connected to the accelerated nucleation of the Mg phase in the MgH_2 matrix: the interface between the Nb:H nanoclusters and the MgH_2 matrix favours the instantaneous nucleation of the Mg phase (heterogeneous nucleation). An embryo of the Mg phase can reduce its energetic formation cost at the MgH_2-Nb:H interface as discussed in general framework; see [26, 27]. In addition, the MgH_2-Nb:H interface can favour the Mg phase growth. Indeed, in diffusional phase

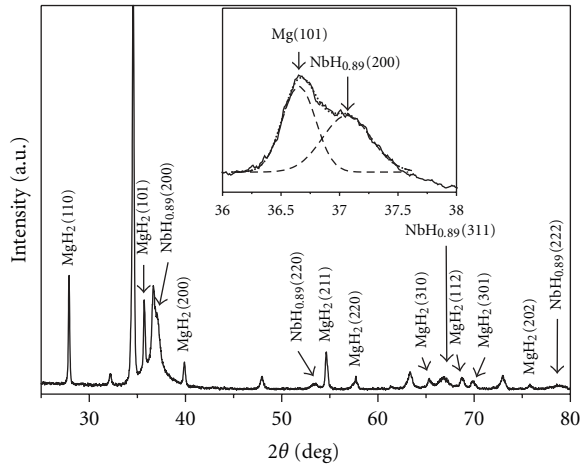

Figure 4: XRD spectrum of the 5 at.% Nb-doped MgH_2 sample, partially dehydrogenated. The inset shows the deconvolution of the Mg (101) and $NbH_{0.89}$ (200) peaks: continuous line: experimental data, dashed line: fitting, and dotted line: envelope of the fitted curves.

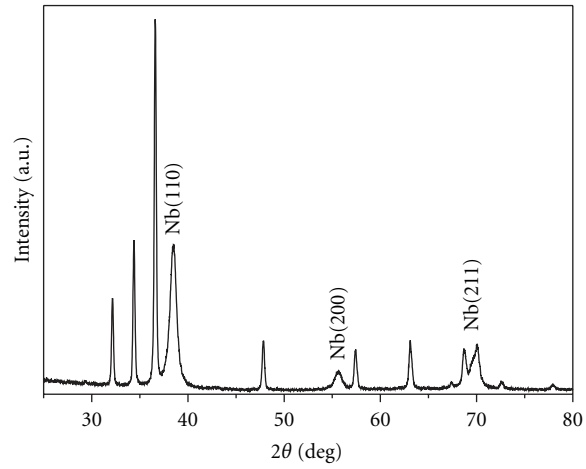

Figure 5: XRD spectrum of the dehydrogenated 5 at.% Nb-doped samples.

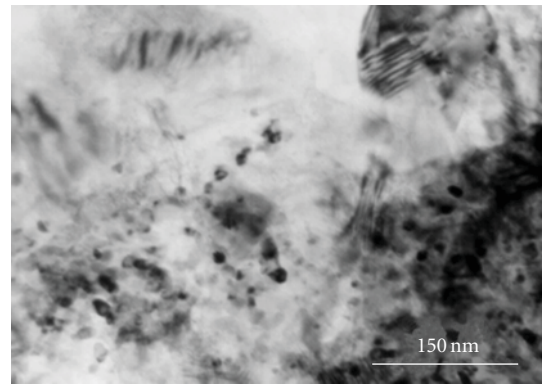

Figure 6: TEM micrograph of the dehydrogenated sample showing distribution and size of the metallic Nb nanoclusters.

transitions where transport of the atomic components occurs over paths longer than the interatomic distance, new phases are often observed to nucleate at grain boundaries of the parent phase. These extended defects result in fast diffusion channels for migrating atoms thus giving rise, in the lattice layers around them, to the critical solute concentration for the phase transition [26, 27]. In the present Nb-doped MgH_2 samples, the MgH_2-Nb:H interface can play a similar role allowing an effective removal of the H atoms dissociated from adjacent MgH_2 layers and thus favouring the formation of Mg nuclei having critical size.

4. Comparison between Desorption Kinetics of Nb-, Zr-, and Fe-Doped MgH_2

In this section we present a comparative study on the H_2 desorption from the MgH_2 matrix doped with different metallic elements dispersed in atomic concentration, say, 2–5 at.% [13]. Results on Nb were reported above and now we consider, for comparison, Fe and Zr because (i) they are transition metals (TM) with catalytic properties for the H_2 sorption kinetics in Mg and (ii) they do not form binary phases with Mg and show negligible solubility [23]. Nb, Zr, and Fe have different "affinity" with hydrogen in the temperature range ($400\,K < T < 700\,K$). Nb forms interstitial alloys with hydrogen: the α phase is a random interstitial alloy of H in bcc Nb with H/Nb ratio <0.31. Zr forms stable phase: the δ phase having fcc structure with $1.31 < H/Nb < 2$. Fe does not form any binary hydride phase and shows negligible H solubility [28]. In these new composite samples, the atomic % concentration, as detected by EDS, was ~5 at.% for Fe (the same as for Nb) and ~3 at.% for Zr: these concentrations are larger than the maximum solubility of the TM in Mg, 0.00043 at.% for Fe at the eutectoid temperature of 920 K, close to 1.3×10^{-4} for Nb in liquid Mg at 1500 K, and lower than 0.1 at.% for Zr at temperatures lower than 700 K [23]. These equilibrium properties indicate that precipitation of the metal additive atoms is expected upon the thermal treatment leading to the sample activation at 623 K and/or during H_2 cycling.

The room temperature XRD spectra of the TM-doped samples, partially dehydrogenated, confirm cluster formation. While Fe remains in the metallic state, see Figure 7, Nb and Zr form hydride phase as shown by the $NbH_{0.89}$ and $ZrH_{1.66}$ reflection peaks in Figures 8 and 9, respectively: no evidence of metallic Nb or Zr was found in the partially desorbed samples. The obtained TM-H phases are appropriate to equilibrium phase diagram at room temperature [28]. The Debye-Scherrer analysis of the XRD peak indicates the formation of TM nanoclusters having dimensions in the $10 \div 20$ nm range while Mg and MgH_2 maintain the microcrystalline structure [9–11]. The aggregation of TM atoms to form nanoclusters during cycling in hydrogen is confirmed by the evolution of XRD spectra from as-deposited to fully cycled samples [9, 11] and by also comparing with EXAFS analysis [11].

In Figure 10 we present the isothermal H_2 desorption curves of the pure and metal-doped MgH_2 samples at the

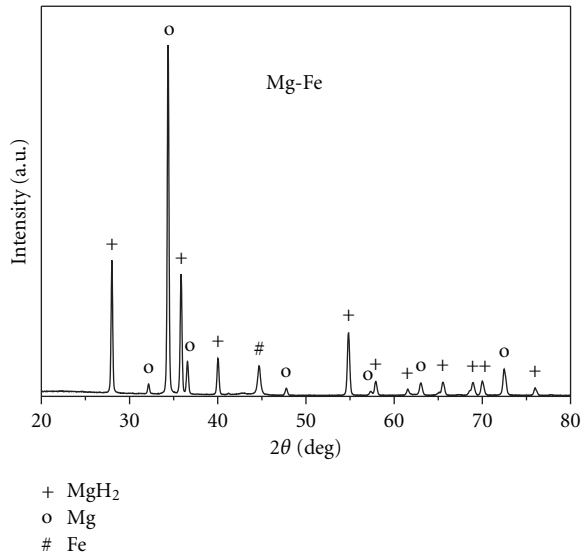

Figure 7: Room temperature XRD spectra of the 5 at.% Fe doped MgH_2 samples, partially dehydrogenated after full activation.

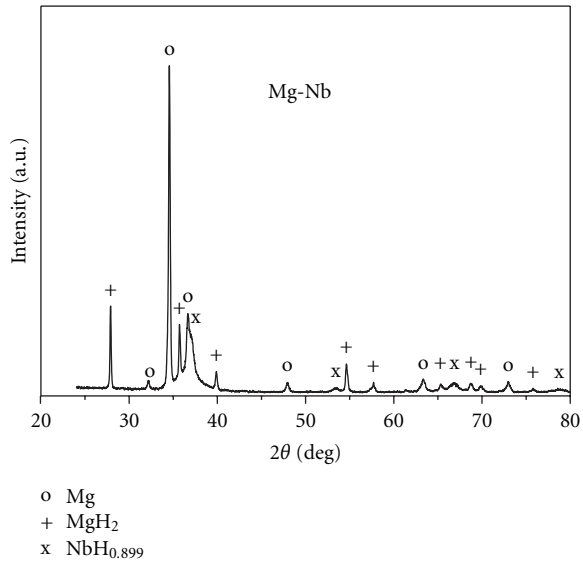

Figure 8: Room temperature XRD spectra of the 5 at.% Nb-doped MgH_2 samples, partially dehydrogenated after full activation.

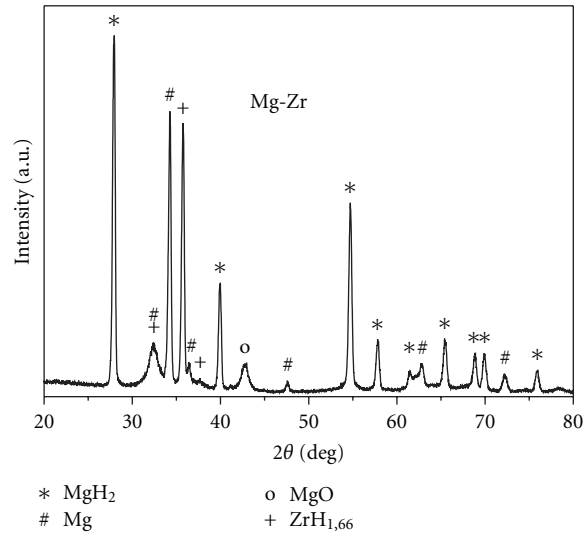

Figure 9: Room temperature XRD spectra of the 3 at.% Zr-doped MgH_2 samples, partially dehydrogenated after full activation.

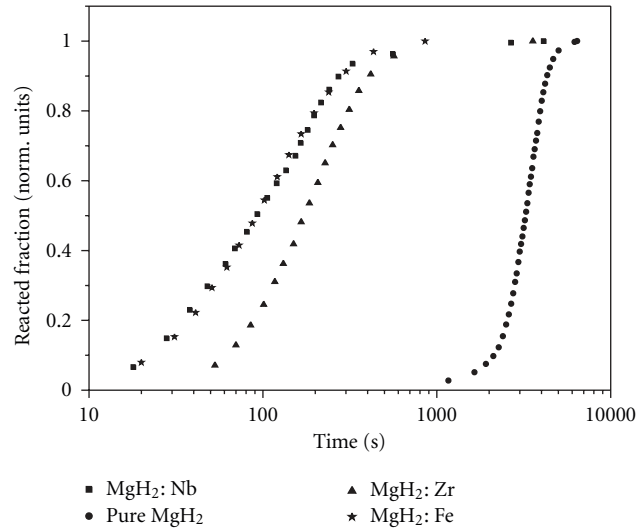

Figure 10: Isothermal H_2 desorption curves of the pure and TM-doped MgH_2 samples at 623 K, after their fully activation.

representative temperature of 623 K. The curves show a strong improvement of the H_2 desorption kinetics in the examined TM-doped samples when compared to the pure MgH_2: at this temperature the interval time required for 50% transformation decreases from ~3000 s for pure MgH_2, to ~200 s for the Zr-doped sample, and to ~100 s for Nb- and Fe-doped samples.

In Figure 11 we present the TDS spectra of the pure and TM-doped MgD_2 samples after their complete activation. (For the TDS analysis deuterium was chosen rather than hydrogen to improve the signal-to-noise ratio: at 2% of the TDS peak height the signal-to-noise ratio of the $m/e = 4$ signal was better than 10^2).

The most important information provided by the spectra is the position of the peak temperature T_P at which the desorption rate reaches its maximum: this temperature allows a direct comparison of the influence of the TM additive on the thermal stability of the MgD_2 phase. The obtained spectra confirm the trend observed in the isothermal curves evidencing lower thermal stability of the TM-doped samples as compared to pure MgD_2. The Fe- and Nb-doped sample show TDS peaks at ~470 and ~480 K, respectively while the Zr-doped samples shows TDS peak at ~535 K. Pure MgD_2shows the TDS peak at a larger temperature, close to 630 K.

The present H_2 (or D_2) desorption results show that the dispersion of different TM nanoclusters inside the MgH_2 matrix accelerates the H_2 desorption process and that TM

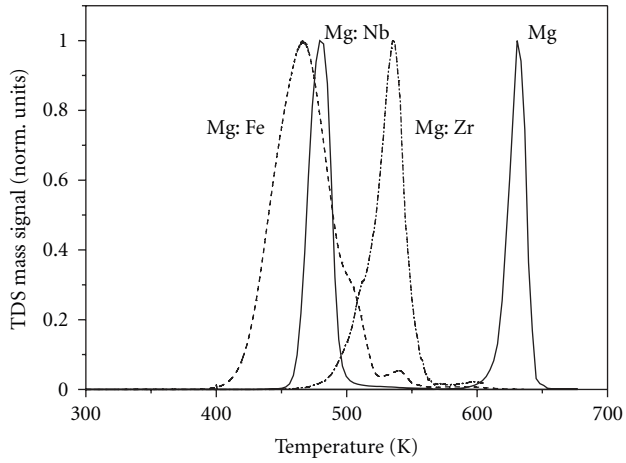

Figure 11: TDS spectra of the pure and TM-doped MgD_2 samples after their fully activation.

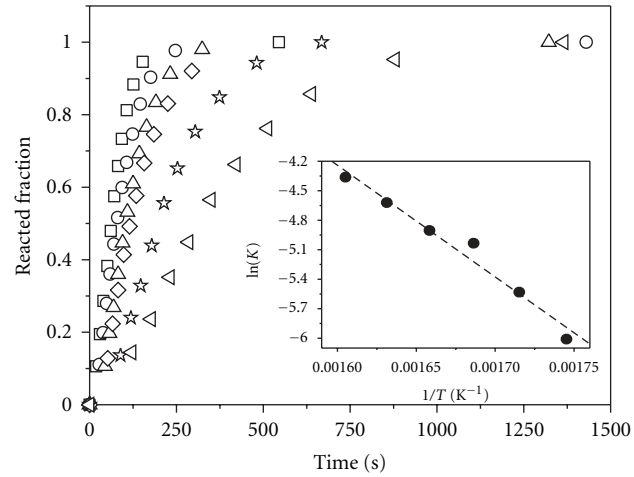

Figure 12: Dehydrogenated fraction versus time at various temperatures for the Mg sample with mixed Fe-Zr additives at □ 623 K, O 613 K, △ 603 K, ◊ 593 K, ⋆ 583 K, and ◁ 573 K. In the insert we present the Arrhenius plot of the desorption rate constant k: the straight line is the least square fit.

nanoclusters distributed in the MgH_2 matrix catalyse the Mg phase nucleation even if they present different chemical affinity with hydrogen. This point is also confirmed by the strong reduction of the nucleation time (Figure 10) shown by the isothermal desorption curves of the TM doped samples (~10 s for Nb and Fe and ~50 s for Zr) as compared to that pertinent to the pure MgD_2, ~1000 s.

In conclusion, composite materials consisting on TM-doped Mg (TM: Nb, Fe, and Zr) with TM content of a few at.% concentration show accelerated H_2 desorption kinetics when compared to the pure MgH_2 samples (the diffusion of migrating hydrogen atoms has been measured by "in situ" EXFAS for the MgH_2/Nb_2O_5 system [29]); while in the pure MgH_2 the H_2desorption kinetics is controlled by the nucleation and growth of the Mg phase, in TM-doped samples the H_2 release is controlled by the H diffusion through Mg layers. The improved H_2 desorption kinetics can be explained by the presence of extended interfaces between MgH_2 and TM nanoclusters acting as heterogeneous sites for the nucleation of the Mg phase and promoting the formation of fast diffusion channels for H migrating atoms.

5. Mixed Zr-Fe Catalysts

In the previous sections we observed that the presence of TM nanoclusters dispersed in the MgH_2 matrix accelerates the H desorption kinetics. Two additional effects were also evidenced by the experiments [12]. First, in Mg samples with Nb content in the at.% level, the hydrogen desorption kinetics, when Nb does not form precipitates, was faster than that observed in the activated sample where Nb forms nanoclusters. Second, catalytic effects were also observed when the metallic additive was present at levels lower than 0.1 at.% in the Mg matrix, that is, close to the solubility limit of Nb in Mg. The desorption curves presented the same kinetics (nucleation and growth mechanisms) and activation energy as that of the pure MgH_2 samples but a shorter nucleation time: we thus suggested that also Nb atoms (or few-atom aggregates) dispersed in the Mg matrix act as nucleation centres for the Mg phase in the parent MgH_2 phase [12].

These results suggest that a route to accelerate the H_2 desorption kinetics is to limit the aggregation of the additives in form of large clusters and to favour a better distribution of the catalyst in form of small clusters or few atoms aggregates into the MgH_2 matrix. To this purpose we have prepared MgH_2 samples with mixed TM additives: in this section we report on the hydrogen desorption from magnesium hydride samples containing Fe and Zr, at a few at.% concentration [14].

We have used Zr and Fe because they have catalytic effects when dispersed in form of nanocluster in the MgH_2 matrix and because they do not form binary phases with Mg matrix. Finally Zr is heavier than Fe and has larger atomic diameter, 4.32 versus 3.44 Å: they thus have different mobility values and we thus expect different clustering processes when sharing the same host matrix (Mg).

The Fe atoms will preferentially form clusters thus limiting the aggregation process of Zr atoms because Fe atoms can faster reach extended defects in the Mg (or MgH_2) matrix which are the typical nucleation centers. To experimentally study this process we prepared Mg samples with (i) Fe single additive (5 at.%), (ii) Zr single additive (3 at.%), and (iii) mixed additive with 7 at.% (~5 and ~2 at.% content for Fe and Zr, resp.).

XRD analysis of the as-deposited samples showed no evidence of metallic Fe and Zr: this means that the presence of the additive is in atomic form or in form of a few atoms aggregates as previously observed with Mg samples containing the Nb additive [11]. Based on previous XRD analysis of TM-doped Mg, it is really difficult to suppose the presence of metallic amorphous phase. In Figure 12 we report the H_2 desorption data pertinent to fully activated MgH_2 samples with Fe-Zr mixed additive [18]. For comparison in Figure 13 we present the H_2 desorption data at the representative

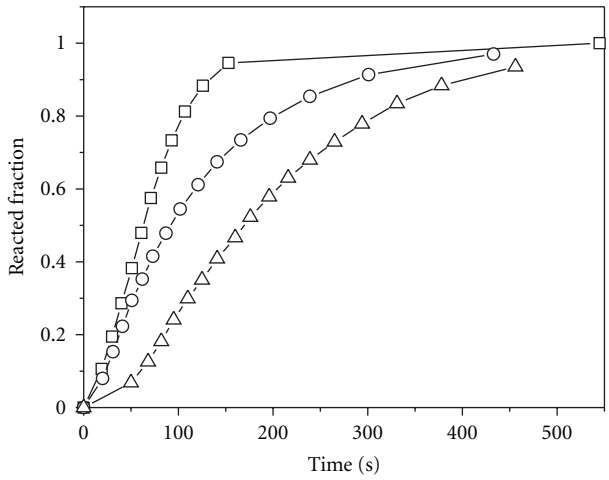

Figure 13: Dehydrogenated fraction versus time at 623 K of MgH_2 sample with Zr (△) and Fe (◯) single additive and mixed Fe-Zr additives (□). The lines are only guide for the eyes.

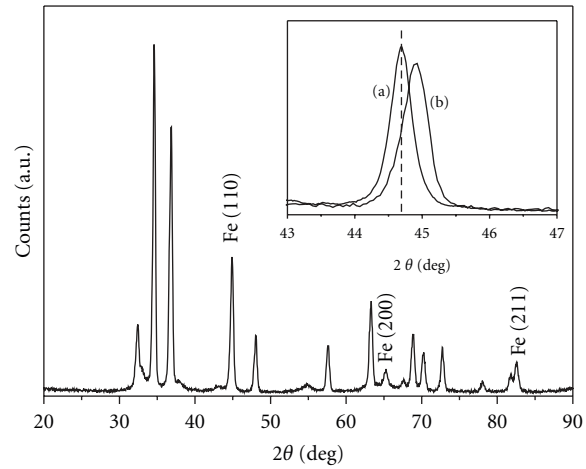

Figure 14: XRD spectra pertinent to Mg samples with mixed Fe-Zr additives (completely activated) after H_2 desorption: in the figure only the Fe reflection peaks are labelled and all others peaks are pertinent to h-Mg reflections. In the inset we present the Fe (110) reflection peak pertinent to a sample with only the Fe additive, line (a), and to a sample with mixed Fe-Zr additives, line (b). The thick line is the reference position of the Fe (110) peak [ICDD 06-0696].

temperature of 623 K pertinent to the MgH_2 samples with single catalyst: symbols (△) for Zr, symbols (◯) for Fe. Symbols (□) are pertinent to the sample with Fe-Zr mixed additives.

In Table 3 we report the kinetic parameters pertinent to samples containing the mixed additives and, as reference, those pertinent to samples with a single additive and to pure MgH_2. We note that in presence of mixed additives the hydride to metal phase transition obeys a nucleation-and-growth mechanism while in presence of a single catalyst (5 at.% Fe or 5 at.% Nb) the phase transformation has diffusive character as shown by the different values of the reaction order n and of activation energy E_a. The most important result is the fact that the mixed additives induce faster desorption kinetic as compared to pure MgH_2 and to $MgH_2$with Fe or Nb as single additive as shown by the $\tau_{1/2}$ parameter. Table 3 also indicates that the hydride decomposition kinetic with mixed additives is very similar to that of the sample with 1 at.% Nb reported in Section 2: the order of reaction is the same, and the activation energy values are very similar. The much better catalytic effect of the mixed additives is related to the impressive increase of pre-exponential factor (A) growing from $\sim 10^4$ to $\sim 10^8$ sec^{-1}. We remark that the improved kinetics compared to that of the sample with single Fe or Zr additive cannot be attributed to the larger additive content because there is a saturation effect in the desorption catalysis with additive contents of ~2 at.% [12].

In Figure 14 we present the XRD spectrum of a fully activated sample after H_2 desorption that provides information on the physical state of the Fe and Zr additives. In the spectrum we observe reflection peaks pertinent to Mg and the (110), (200), and (211) Bragg reflections of the α-Fe phase but no XRD peak attributable to Zr nor to any Fe-Zr phase. Because Zr and Fe as single additive cannot produce the fast desorption kinetics shown in Figure 12, we may suppose that the improved catalytic effect of the mixed additives has two causes: (i) aggregation of Fe into nanoclusters and (ii) atomic dispersion of Zr (that could also form aggregates but consisting on few atoms). We remark that the second effect has permanent character because, contrarily to the samples with single additive, no evidence of Zr clustering is observed also after repeated H_2 sorption cycles.

By using the Williamson-Hall method [30] the size of the α-Fe crystallites was determined to be lower than 20 nm. We can also evaluate a low microstrain value of $\varepsilon \sim 6 \times 10^{-4}$ not observed in the Mg sample with single Fe additive. The intensity ratio of these diffraction peaks indicates that the α-Fe nanoclusters have a random distribution in the Mg matrix. The α-Fe clusters size is lower than in Mg samples with single Fe additive, ~30 nm, as evaluated by the Bragg-Brentano analysis of the (110) reflection peak presented in the inset of Figure 14, line (a) (this is the only α-Fe reflection in the XRD spectrum). Both samples have the same Fe content, ~5 at.%, and assuming that all Fe atoms form precipitates, we conclude that the sample with mixed additives presents a higher Fe cluster density.

In the Mg sample with Zr as single additive, after segregation upon diffusion, Zr atoms aggregate forming clusters [13]. In the sample with mixed additives these Zr clusters are not observed: the larger Fe mobility suggests that a possible mechanism impeding the Zr aggregation is the Fe clustering in the disposable nucleation centres which anticipates the Zr precipitation. The lower size of the Fe clusters in the Mg sample with mixed additives can be explained by a larger density of available nucleation sites as compared to that in the Mg sample with single Fe additive: reasonably, the Zr few-atom aggregates may constitute precipitation centres for Fe atoms.

Table 3: Evaluated values of the half-reaction time ($\tau_{1/2}$) at $T = 623$ K, order of reaction (n), activation energy (E_a), and pre-exponential factor (A) of pure and TM-doped (TM: Nb, Fe, and Zr + Fe) MgH_2 samples.

Sample	$\tau_{1/2}$ (s)	n	E_a (kJ mol^{-1}H)	A (s^{-1})
Pure Mg	3250 ± 50	4	141 ± 5	$\sim 10^8$
Mg + 5 at.% Nb	110 ± 10	1	51 ± 5	$\sim 10^2$
Mg + 1 at.% Nb	290 ± 10	1.5	78 ± 5	$\sim 10^4$
Mg + 5 at.% Fe	100 ± 10	1	51 ± 5	$\sim 10^2$
Mg + (Fe-Zr)	70 ± 10	1.5	94 ± 5	$\sim 10^8$

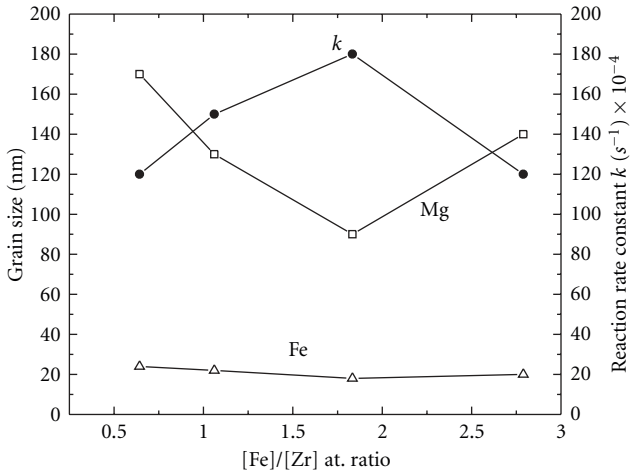

Figure 15: Fe cluster size (triangles), Mg grain size (squares) and desorption rate constant (circles) at different [Fe]/[Zr] atomic ratios. The lines are only a guide for the eye.

To gain a deeper understanding on the kinetic processes in presence of mixed additives and to determine which is the optimum Fe and Zr atomic concentrations, we have prepared samples with fixed metal content, about 7 at.%, by changing the [Fe]/[Zr] atomic ratio [31]. In Figure 15 we summarize the results by showing the size of the Fe nanoclusters, the Mg grain size, and the desorption rate constant k ($T = 623$ K) as function of the [Fe]/[Zr] ratio. From Figure 15 we observe that (i) the H_2 desorption rate constant attains its maximum value when the [Fe]/[Zr] atomic ratio is ∼1, (ii) Fe forms nanoclusters with 20 nm grain size independently on the [Fe]/[Zr] atomic ratio, (iii) at [Fe]/[Zr] ∼1.8 the Mg grain size attains its minimum value of about 100 nm, and (iv) there is not evidence of Zr atoms aggregates.

To explain the previous results, we suggest that the synergetic effect of the mixed Fe and Zr additives consists of (i) Fe aggregation forming nanosized clusters that act as Mg nucleation centers and promote the formation of interconnected Mg domains for fast H diffusion and (ii) Zr atoms playing most probably a role by favoring and stabilizing the aggregation of the Fe additive and as Mg grain refiner by limiting Mg grain growth [32]: grain refinement certainly contributes to increase kinetic favoring diffusion through grain boundaries.

In the future it would be interesting to investigate the possible existence of correlation effects on diffusion when different dopants are moving and clustering occurs as observed in [33].

6. Conclusions

We have studied the hydrogen desorption kinetics of TM-doped MgH_2 samples to analyse the catalytic role of TM atoms and nanoparticles dispersed into the magnesium hydride matrix. We observed that (i) TMs are able to enhance hydrogen desorption also at very low concentration (0.06 at.%) which means that they are atomically dispersed or form a few-atom aggregates, (ii) TM-doped samples show stable desorption properties after a number of H_2 sorption cycles when TM nanoclusters are formed with radius on the order of 10–20 nm, and (iii) mixed TM (in the present case Fe and Zr) can further enhance the desorption kinetics as compared to the single additive.

The improved H_2 desorption properties of the single TM additive are explained by the presence of interfaces between the MgH_2 and the TM nanoclusters acting as heterogeneous nucleation sites and promoting the formation of fast diffusion channels for H migrating atoms. In our case mixed TM (Fe-Zr) additive in the Mg matrix optimizes the distribution and size of TM nanoclusters contained inside the MgH_2 matrix.

PACS

64.70.K-: Solid–solid transitions
61.46.+w: Nanoscale materials: clusters, nanoparticles, nanotubes and nanocrystals
61.05.C-: X-ray diffraction and scattering
68.37.Lp: Transmission electron microscopy (TEM)
68.43.Nr: Desorption kinetics
68.43.Vx Thermal desorption
81.05.-t: Specific materials: fabrication, treatment, testing, and analysis
82.65.+r: Surface and interface chemistry; heterogeneous catalysis at surfaces
84.60.Ve: Energy storage systems, including capacitor banks.

Acknowledgments

The authors thank Cristina Armellini for XRD analysis, Chiara Maurizio for EXAFS analysis, Paolo Mengucci for TEM analysis, Paolo Mazzoldi and Cinzia Sada for SIMS analysis, Romina Belli for EDS analysis, and Ashwin Kale

for support on Mg samples preparation with mixed TM additives. The research activity is financially supported by the Hydrogen-FISR Italian Project.

References

[1] R. Gonzalez, Y. Chen, and K. L. Tsang, "Diffusion of deuterium and hydrogen in doped and undoped MgO crystals," *Physical Review B*, vol. 26, no. 8, pp. 4637–4645, 1982.

[2] O. Friedrichs, J. C. Sánchez-López, C. López-Cartes et al., "Chemical and microstructural study of the oxygen passivation behaviour of nanocrystalline Mg and MgH2," *Applied Surface Science*, vol. 252, no. 6, pp. 2334–2345, 2006.

[3] G. Friedlmeier and M. Groll, "Experimental analysis and modelling of the hydriding kinetics of Ni-doped and pure Mg," *Journal of Alloys and Compounds*, vol. 253-254, pp. 550–555, 1997.

[4] A. Zaluska, L. Zaluski, and J.O. Ström-Olsen, "Structure, catalysis and atomic reactions on the nano-scale: a systematic approach to metal hydrides for hydrogen storage," *Applied Physics A*, vol. 72, no. 2, pp. 157–165, 2001.

[5] G. Barkhordarian, T. Klassen, and R. Bormann, "Catalytic mechanism of transition-metal compounds on Mg hydrogen sorption reaction," *Journal of Physical Chemistry B*, vol. 110, no. 22, pp. 11020–11024, 2006.

[6] J. F. Pelletier, J. Huot, M. Sutton et al., "Hydrogen desorption mechanism in MgH2-Nb nanocomposites," *Physical Review B*, vol. 63, no. 5, Article ID 052103, pp. 1–4, 2001.

[7] H. G. Schimmel, J. Huot, L. C. Chapon, F. D. Tichelaar, and F. M. Mulder, "Hydrogen cycling of niobium and vanadium catalyzed nanostructured magnesium," *Journal of the American Chemical Society*, vol. 127, no. 41, pp. 14348–14354, 2005.

[8] O. Friedrichs, J. C. Sánchez-López, C. López-Cartes, T. Klassen, R. Bormann, and A. Fernández, "Nb_2O_5 "pathway effect" on hydrogen sorption in Mg," *Journal of Physical Chemistry B*, vol. 110, no. 15, pp. 7845–7850, 2006.

[9] N. Bazzanella, R. Checchetto, and A. Miotello, "Catalytic effect on hydrogen desorption in Nb-doped microcrystalline MgH2," *Applied Physics Letters*, vol. 85, no. 22, pp. 5212–5214, 2004.

[10] R. Checchetto, N. Bazzanella, A. Miotello, and P. Mengucci, "Deuterium storage in Mg-Nb films," *Journal of Alloys and Compounds*, vol. 404–406, pp. 461–464, 2005.

[11] R. Checchetto, N. Bazzanella, A. Miotello et al., "Nb clusters formation in Nb-doped magnesium hydride," *Applied Physics Letters*, vol. 87, no. 6, Article ID 061904, 3 pages, 2005.

[12] N. Bazzanella, R. Checchetto, A. Miotello, C. Sada, P. Mazzoldi, and P. Mengucci, "Hydrogen kinetics in magnesium hydride: on different catalytic effects of niobium," *Applied Physics Letters*, vol. 89, no. 1, Article ID 014101, 3 pages, 2006.

[13] R. Checchetto, N. Bazzanella, A. Miotello, and P. Mengucci, "Catalytic properties on the hydrogen desorption process of metallic additives dispersed in the MgH2 matrix," *Journal of Alloys and Compounds*, vol. 446-447, pp. 58–62, 2007.

[14] N. Bazzanella, R. Checchetto, and A. Miotello, "Catalytic effect of mixed Zr-Fe additives on the hydrogen desorption kinetics of MgH_2," *Applied Physics Letters*, vol. 92, no. 5, Article ID 051910, 2008.

[15] R. Checchetto, N. Bazzanella, A. Miotello, R. S. Brusa, A. Zecca, and A. Mengucci, "Deuterium storage in nanocrystalline magnesium thin films," *Journal of Applied Physics*, vol. 95, no. 4, pp. 1989–1995, 2004.

[16] M. A. Pick, J. W. Davenport, M. Strongin, and G. J. Dienes, "Enhancement of hydrogen uptake rates for Nb and Ta by thin surface overlayers," *Physical Review Letters*, vol. 43, no. 4, pp. 286–289, 1979.

[17] R. Checchetto, G. Trettel, and A. Miotello, "Sievert-type apparatus for the study of hydrogen storage in solids," *Measurement Science and Technology*, vol. 15, no. 1, pp. 127–130, 2004.

[18] J. W. Christian, *The Theory of Transformations in Metals and Alloys. Part I*, Pergamon, Oxford, UK, 2002.

[19] J. Renner and H. J. Grabke, "Determination of diffusion coefficients in the hydriding of alloys," *Zeitschrift fuer Metallkunde*, vol. 69, no. 10, pp. 639–642, 1978.

[20] G. Liang, J. Huot, S. Boily, A. Van Neste, and R. Schulz, "Catalytic effect of transition metals on hydrogen sorption in nanocrystalline ball milled MgH_2-Tm (Tm = Ti, V, Mn, Fe and Ni) systems," *Journal of Alloys and Compounds*, vol. 292, no. 1-2, pp. 247–252, 1999.

[21] G. Barkhordarian, T. Klassen, and R. Bormann, "Kinetic investigation of the effect of milling time on the hydrogen sorption reaction of magnesium catalyzed with different Nb_2O_2 contents," *Journal of Alloys and Compounds*, vol. 407, no. 1-2, pp. 249–255, 2006.

[22] J. F. Fernández and C. R. Sánchez, "Rate determining step in the absorption and desorption of hydrogen by magnesium," *Journal of Alloys and Compounds*, vol. 340, no. 1-2, pp. 189–198, 2002.

[23] A. A. Nayeb-Hashemy and J. B. Clark, *Phase Diagrams of Binary Magnesium Alloys*, ASM International, Metal Park, Ohio, USA, 1988.

[24] G. Alefeld and J. Völkl, *Hydrogen in Metals*, Springer, Berlin, Germany, 1978.

[25] M. A. Pick and R. Bausch, "The determination of the force-dipole tensor of hydrogen in niobium," *Journal of Physics F*, vol. 6, no. 10, article no. 008, pp. 1751–1763, 1976.

[26] D. A. Porter and K. E. Easterling, *Phase Transformation in Metals and Alloys*, Chapmann & Hall, London, UK, 1992.

[27] D. Turnbull, *Solid State Physics*, vol. 3, Academic Press, New York, NY, USA, 1956.

[28] F. D. Manchester, *Phase Diagrams of Binary Hydrogen Alloys*, ASM International, Materials Park, Ohio, USA, 2000.

[29] O. Friedrichs, D. Martínez-Martínez, G. Guilera, J. C. S. López, and A. Fernández, "In situ energy-dispersive XAS and XRD study of the superior hydrogen storage system MgH_2/Nb_2O_5," *Journal of Physical Chemistry C*, vol. 111, no. 28, pp. 10700–10706, 2007.

[30] G. K. Williamson and W. H. Hall, "X-ray line broadening from filed aluminium and wolfram," *Acta Metallurgica*, vol. 1, no. 1, pp. 22–31, 1953.

[31] A. Kale, N. Bazzanella, R. Checchetto, and A. Miotello, "Synergy on catalytic effect of Fe-Zr additives mixed in different proportions on the hydrogen desorption from MgH_2," *Applied Physics Letters*, vol. 94, no. 20, Article ID 204103, 2 pages, 2009.

[32] E. F. Emley, *Principles of Magnesium Technology*, Pergamon, Oxford, UK, 1966.

[33] A. Miotello, G. De Marchi, G. Mattei, P. Mazzoldi, and C. Sada, "Clustering of gold atoms in ion-implanted silica after thermal annealing in different atmospheres," *Physical Review B*, vol. 63, no. 7, Article ID 075409, 7 pages, 2001.